A Mechanism for Turing Pattern Formation with Active and Passive Transport[*]

Heather A. Brooks[†] and Paul C. Bressloff[†]

Abstract. We propose a novel mechanism for Turing pattern formation that provides a possible explanation for the regular spacing of synaptic puncta along the ventral cord of *C. elegans* during development. The model consists of two interacting chemical species, where one is passively diffusing and the other is actively trafficked by molecular motors. We identify the former as the kinase CaMKII and the latter as the glutamate receptor GLR-1. We focus on a one-dimensional model in which the motor-driven chemical switches between forward and backward moving states with identical speeds. We use linear stability analysis to derive conditions on the associated nonlinear interaction functions for which a Turing instability can occur. We find that the dimensionless quantity $\gamma = \alpha d/v^2$ has to be sufficiently small for patterns to emerge, where α is the switching rate between motor states, v is the motor speed, and d is the passive diffusion coefficient. One consequence is that patterns emerge outside the parameter regime of fast switching where the model effectively reduces to a two-component reaction-diffusion system. Numerical simulations of the model using experimentally based parameter values generates patterns with a wavelength consistent with the synaptic spacing found in *C. elegans*. Finally, in the case of biased transport, we show that the system supports spatially periodic patterns in the presence of boundary forcing, analogous to flow distributed structures in reaction-diffusion-advection systems. Such forcing could represent the insertion of new motor-bound GLR-1 from the soma of ventral cord neurons.

1. Introduction. Pattern formation and symmetry breaking is a question of great theoretical and experimental interest. While the study of morphogenesis has a rich history, perhaps the most well-known contribution is the 1952 paper of Alan Turing [34]. In this classical work, Turing suggested two necessary parts of pattern formation: two (or more) interacting chemical species, with different rates of diffusion for the participating species. Turing derived conditions such that the combination of nonlinear reaction kinetics and diffusion can lead to instability of the homogeneous steady state. These instabilities are known as Turing patterns. Gierer and Meinhardt [8] highlighted one important general example where these conditions hold, namely, that the system involves a short-range activator and a long-range inhibitor. Turing patterns in reaction-diffusion equations are well understood and have been studied in a variety of contexts, including biology, chemistry, and physics [20].

[†]Department of Mathematics, University of Utah, Salt Lake City, UT 84112-0090 (heather@math.utah.edu, bressloff@math.utah.edu).

While interest in Turing pattern formation was initially primarily theoretical, there is an ever expanding literature on applications and extensions. Reaction-diffusion mechanisms have been implicated in the development of feather patterns, vertebrate skin patterns, seashells [17], and zebrafish stripes [36], as well as limb development [1] and ocular dominance stripes [33]. In addition, there have been many efforts to expand the understanding of conditions beyond the traditional reaction-diffusion paradigm under which patterns may form. To give a few examples, Turing-type patterns have been shown to form on growing domains [5], via a signal transduction mechanism [25], and via mechanical instability [10]. In this paper, we further extend this literature by proposing a novel mechanism for Turing pattern formation, which is driven by two interacting chemical species, where one is passively diffusing and the other is being actively trafficked by molecular motors.

The biological motivation underlying our proposed active trafficking mechanism for Turing pattern formation comes from cellular biology, in particular, the observation that there is a regularly spaced distribution of ventral cord and dorsal cord synapses in *Caenorhabditis elegans*, as illustrated in Figure 1. There is growing experimental evidence that synaptogenesis involves the regulation of the active (kinesin-based) transport and delivery of glutamate receptors (GLR-1) to synapses by type II calcium- and calmodulin-dependent protein kinase (CaMKII) [26, 11, 12]; see Figure 2. First, the activation (autophosphorylation) of CaMKII via voltage-gated calcium channels induces the formation of new synapses by enhancing the active transport and delivery of GLR-1 to developing synaptic sites. On the other hand, the resulting increase in excitation arising from the increase in membrane-bound receptors leads to the synaptic delocalization of active CaMKII due to increased calcium levels. This is consistent with the observation that the synaptic localization of CaMKII changes in response to autophosphorylation [31]. In this paper, we show how a regular spacing of synapses can be established in *C. elegans* via an underlying Turing mechanism for synaptogenesis involving a short-range activator and a long-range inhibitor. We identify the former as slowly diffusing CaMKII and the latter as a rapidly advecting GLR-1, which switches between anterograde and retrograde motor-driven transport (bidirectional transport). Our Turing mechanism is novel, since the inhibitor does not diffuse.

The outline of this paper is as follows. In section 2 we formulate a three-component (two chemical species), one-dimensional (1D) model of synaptogenesis in *C. elegans*, with
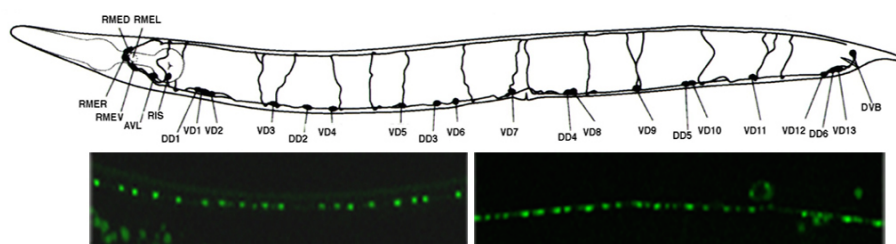
Figure 1. *Schematic figure showing distribution of synapses of the type D motor neurons. The D type neurons include six DD and 13 VD neurons. DD form synapses to the dorsal body muscles and VD form synapses to the ventral muscles. Blobs: synapses to muscles; arrows: synaptic inputs to the D neurons. Below are GFP images of synaptic puncta in the dorsal and ventral cords, respectively. (Public domain figure downloaded from WormBook/Synaptogenesis by Y. Jin, http://www.wormbook.org/.)*
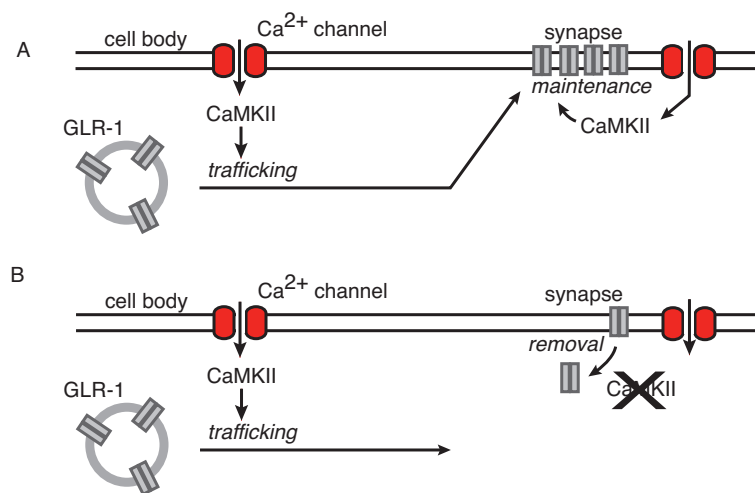
Figure 2. *Regulation of transport and delivery of GLR-1 to synapses by CaMKII. (A) Calcium influx through voltage-gated calcium channels activates CaMKII, which enhances the active transport and delivery of GLR-1 to synapses. (B) Under conditions of increased excitation, higher calcium levels result in active CaMKII which fails to localize at synapses, leading to the removal of GLR-1 from synapses.*

an activator CaMKII moving only via diffusion and an inhibitor GLR-1 traveling by active (motor-driven) transport in either the leftward or rightward direction. We take the reaction kinetics of the two chemical species to be based on a modified Gierer–Meinhardt model [8], since CaMKII exhibits autophosphorylation. We then use linear stability analysis to derive conditions for a Turing instability and construct dispersion curves (section 3). It could be argued that occurrence of patten formation in our transport model is not particularly surprising, since one might be inclined to interpret switching between left and right moving states as effectively equivalent to diffusion. However, this equivalence holds only in the limit of fast switching, and we show that this lies outside the pattern forming regime of our model. In section 4 we break the symmetry between the left- and right-moving active particles by taking their speeds to be different. This biased transport model reduces to a reaction-diffusion-advection (RDA) model in the fast switching limit. We show that the full system supports spatially periodic flow-distributed structures (FDS) on a semi-infinite domain with boundary forcing, analogous to what is found in RDAs [30]. Finally, in section 5 we highlight extensions to this work and future areas of research.

2. Three-component trafficking model. Consider a 1D domain of fixed length L, which represents a neurite in the ventral cord of *C. elegans* at a particular stage of larval development; see Figure 3. Let $R(x,t)$ denote the concentration of GLR-1 receptors at position x along the cell at time t and let $U(x,t)$ denote the corresponding concentration of active CaMKII. For simplicity, we do not distinguish between membrane-bound and cytoplasmic densities. Within the context of synaptogenesis, we will interpret steady-state regions of enhanced densities in GLR-1 and CaMKII as potential synaptic sites. This imposes one constraint on our model, namely, that spatially periodic distributions of CaMKII and GLR-1 are in-phase. (A more detailed model would explicitly take into account the Ca^{2+}-dependent localization of CaMKII
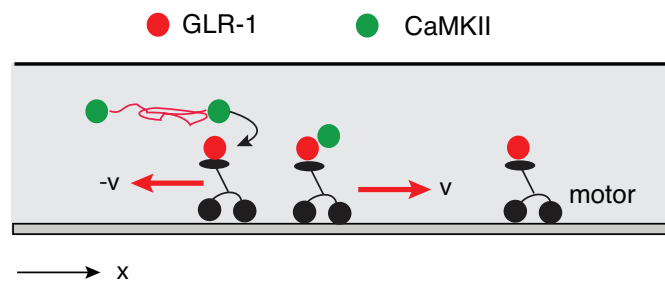
Figure 3. *One-dimensional, three-component trafficking model. Passively transported molecules of CaMKII (green) react with motor-driven actively transported molecules of GLR-1 (red). The latter can switch between forward and backward moving states (traveling with velocities $\pm v$). Interactions between motor-driven particles such as exclusion effects (hard-core repulsion) are ignored.*

at the membrane and the CaMKII-dependent delivery of GLR-1 to developing synaptic sites.) We partition GLR-1 into two subpopulations: those that undergo anterograde (rightward) transport with positive velocity v and density $R_+(x,t)$ and those that undergo retrograde (leftward) transport with negative velocity $-v$ and density $R_-(x,t)$:

$$(2.1) \qquad R(x,t) = R_+(x,t) + R_-(x,t).$$

(The case of different speeds in the left and right directions will be considered in section 4.) Individual receptors randomly switch between the two advective states according to a two-state Markov process,

$$(2.2) \qquad R_+ \underset{\alpha}{\overset{\alpha}{\rightleftharpoons}} R_-.$$

This is based on the assumption that actively transported particles (ATs) are transported bidirectionally along a microtubule or actin filament by some motor complex [3]. We take the various concentrations to evolve according to the system of equations

$$(2.3a) \qquad \frac{\partial U}{\partial t} = D\frac{\partial^2 U}{\partial x^2} + f(U, R_+, R_-),$$

$$(2.3b) \qquad \frac{\partial R_+}{\partial t} = -v\frac{\partial R_+}{\partial x} - \alpha R_+ + \alpha R_- + g(U, R_+, R_-),$$

$$(2.3c) \qquad \frac{\partial R_-}{\partial t} = v\frac{\partial R_-}{\partial x} + \alpha R_+ - \alpha R_- + g(U, R_+, R_-).$$

The first term on the right-hand side of (2.3a) represents diffusive transport of CaMKII and the first term on the right-hand side of (2.3b) and (2.3c) represents ballistic transport of GLR-1 to the right or left, respectively. The terms $\pm\alpha(r-l)$ represent the effects of switching between the two advective states. The reaction term f represents both the autocatalysis of CaMKII and the inhibition of CaMKII by GLR-1, whereas the reaction terms g represent
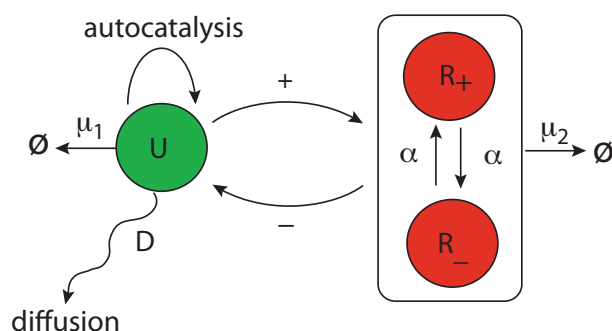
Figure 4. *Schematic diagram of modified Gierer and Meinhardt activator-inhibitor model with a passively diffusing activator (U) and an actively transported inhibitor switching between left (R_-) and right (R_+) moving states at a rate α.*

the increase in actively transported GLR-1 due to the action of CaMKII. Finally, (2.3) are supplemented by reflecting boundary conditions at the ends $x = 0, L$:

$$(2.4) \qquad \left.\frac{\partial U(x,t)}{\partial x}\right|_{x=0,L} = 0, \quad vR_+(0,t) = vR_-(0,t), \quad vR_+(L,t) = vR_-(L,t).$$

It remains to specify the form of the nonlinear reaction functions f and g. Since the precise details of the interaction between CaMKII and GLR-1 are currently not known, we will adapt a classical model of autocatalysis in pattern forming systems due to Gierer and Meinhardt (GM model) [8]. The GM model consists of an activator-inhibitor system with bimolecular activation and monomolecular inhibition; see Figure 4. More specifically, we take

$$(2.5a) \qquad f(U, R_+, R_-) = \frac{\rho U^2}{R_+ + R_-} - \mu_1 U,$$

$$(2.5b) \qquad g(U, R_+, R_-) = \rho U^2 - \mu_2(R_+ + R_-).$$

Here, $\rho > 0$ represents the strength of interactions and μ_1, μ_2 represent the degradation rates of CaMKII and GLR-1, respectively. We are assuming that both left and right GLR-1 have an equal inhibitory effect on CaMKII, and for simplicity we have also taken g to be a symmetric function of $R_\pm$. (This can also be imposed by an appropriate shift in the switching rates; the basic results of the paper do not depend on imposing such a symmetry; see also the discussion of biased transport in section 4.) Another biologically based reason for choosing the GM model is that it generates in-phase patterns for two-component reaction-diffusion systems [20].

3. Conditions for Turing instability in trafficking model. In the following it will be convenient to rescale space and time such that $\hat{x} = \alpha x/v$ and $\hat{t} = \alpha t$, so that (2.3) become (after dropping the hat notation)

$$(3.1a) \qquad \frac{\partial U}{\partial t} = \gamma \frac{\partial^2 U}{\partial x^2} + \frac{1}{\alpha} f(U, R_+, R_-),$$

$$(3.1b) \qquad \frac{\partial R_+}{\partial t} = -\frac{\partial R_+}{\partial x} + R_- - R_+ + \frac{1}{\alpha} g(U, R_+, R_-),$$

$$(3.1c) \qquad \frac{\partial R_-}{\partial t} = \frac{\partial R_-}{\partial x} + R_+ - R_- + \frac{1}{\alpha} g(U, R_+, R_-),$$

where

(3.2)
$$\gamma = \frac{\alpha D}{v^2}$$

is the nondimensional quantity relating the CaMKII diffusion coefficient, GLR-1 velocity, and motor switching rate. As we shall see, γ is the analogue of the ratio of diffusivities in classical reaction-diffusion systems [20].

3.1. Linear stability analysis. We are interested in deriving general conditions for a Turing instability in the system of equations (3.1) and then applying them to the modified GM model for synaptogenesis in *C. elegans*. We will proceed along lines analogous to the classical theory of diffusion-driven pattern formation [20, 7] by linearizing about a spatially uniform fixed point and studying the spectrum of the resulting linear operator. Since neurite length is relatively large compared to the synapse density pattern, the boundaries don't have a major effect on wavelength. Thus, we consider a homogeneous partial differential equation in the unbounded domain $\mathbb{R}$, and the associated spectrum is continuous. However, with a slight abuse of notation, we will still refer to elements $\lambda(k)$, $k \in \mathbb{R}$, of the continuous spectrum as eigenvalues and the associated Fourier components e^{ikx} as eigenfunctions. The goal is to determine conditions under which $\mathrm{Re}[\lambda(0)] < 0$ (stable with respect to homogeneous perturbations), whereas there exists a critical wavenumber k_c such that

$$\max_{k \in \mathbb{R}}\{\mathrm{Re}[\lambda(k)]\} = \mathrm{Re}[\lambda(k_c)] = \lambda(k_c) = 0.$$

Under these conditions, the fixed point is marginally stable with respect to excitation of a spatially periodic pattern of critical wavelength $2\pi/k_c$. Typically, varying one of the parameters of the underlying model can then push the associated dispersion curve $\lambda = \lambda(k)$ above zero in a neighborhood of k_c, resulting in a Turing instability. Whether a stable periodic pattern forms then depends on the nonlinearities of the system, which can be investigated numerically or by using weakly nonlinear analysis. In this paper, we shall treat the dimensionless parameter γ of (3.2) as the bifurcation parameter.

Suppose that there exists a spatially uniform fixed point $\boldsymbol{u}^* = (U^*, R_+^*, R_-^*)$ for which $f(U^*, R_+^*, R_-^*) = g(U^*, R_+^*, R_-^*) = 0$ and $R_+^* = R_-^*$. Linearizing about this fixed point by setting

$$U(x,t) = U^* + u(x,t), \quad R_+(x,t) = R_+^* + r(x,t), \quad R_-(x,t) = R_-^* + l(x,t)$$

yields the linear equation

(3.3)
$$\boldsymbol{u}_t = \mathbf{D}\boldsymbol{u}_{xx} + \mathbf{J}\boldsymbol{u}_x + \frac{1}{\alpha}\mathbf{A}\boldsymbol{u},$$

where $\boldsymbol{u} = (u \quad r \quad l)^T$ and

$$\mathbf{D} = \begin{pmatrix} \gamma & 0 & 0 \\ 0 & 0 & 0 \\ 0 & 0 & 0 \end{pmatrix}, \quad \mathbf{J} = \begin{pmatrix} 0 & 0 & 0 \\ 0 & -1 & 0 \\ 0 & 0 & 1 \end{pmatrix}, \quad \mathbf{A} = \begin{pmatrix} f_u & f_r & f_r \\ g_u & -\alpha + g_r & \alpha + g_r \\ g_u & \alpha + g_r & -\alpha + g_r \end{pmatrix},$$

with all derivatives evaluated at the fixed point. We have used the fact that $f_r = f_l$ and $g_r = g_l$ at the fixed point. In the absence of spatial processes, the linearized system (3.3) reads

$$(3.4) \qquad\qquad \boldsymbol{u}_t = \frac{1}{\alpha}\mathbf{A}\boldsymbol{u},$$

where $\boldsymbol{u}$ has solutions of the form $\boldsymbol{u} \propto e^{\lambda t}$. The eigenvalues λ of this system satisfy

$$0 = -\lambda^3 + \lambda^2\left(-2 + \frac{1}{\alpha}\left(f_u + 2g_r\right)\right)$$
$$+ \lambda\left(\frac{2}{\alpha^2}\left(-f_u g_r + f_r g_u\right) + \frac{2}{\alpha}\left(f_u + 2g_r\right)\right) + \frac{4}{\alpha^2}\left(-f_u g_r + f_r g_u\right).$$

This has solutions

$$(3.5) \qquad\qquad \lambda_1 = -2,$$
$$(3.6) \qquad\qquad \lambda_{2,3} = \frac{1}{2\alpha}\left(f_u + 2g_r \pm \sqrt{\left(f_u + 2g_r\right)^2 - 8\left(f_u g_r - f_r g_u\right)}\right).$$

We require the steady state to be stable in the absence of spatial effects, i.e., $\mathrm{Re}(\lambda) < 0$ for all λ. Conditions for λ to be negative in the absence of spatial components are as follows:

$$(3.7a) \qquad\qquad f_u + 2g_r < 0,$$
$$(3.7b) \qquad\qquad f_u g_r - f_r g_u > 0.$$

Now we consider the stability of the full system with respect to spatially periodic perturbations. We assume (3.3) has a solution of the form $\boldsymbol{u}(x,t) = \boldsymbol{u}_k e^{\lambda t} e^{ikx}$, which gives the matrix equation

$$(3.8) \qquad\qquad \lambda\boldsymbol{u}_k = \Delta(k)\boldsymbol{u}_k, \quad \Delta(k) = -k^2\gamma + ikJ + \frac{1}{\alpha}A.$$

Hence, λ satisfies the characteristic equation

$$0 = \det[\Delta(k) - \lambda I_3] = -\lambda^3 + \lambda^2\left(-2 - \gamma k^2 + \frac{1}{\alpha}\left(f_u + 2g_r\right)\right)$$
$$+ \lambda\left(\frac{2}{\alpha^2}\left(-f_u g_r + f_r g_u\right) + \frac{2}{\alpha}\left(f_u + 2g_r + \gamma g_r k^2\right) - k^2 - 2\gamma k^2\right)$$
$$+ \frac{4}{\alpha^2}\left(-f_u g_r + f_r g_u\right) + \frac{k^2}{\alpha}\left(f_u + 4\gamma g_r\right) - \gamma k^4.$$

This can be written in the more compact form

$$(3.9) \qquad\qquad \lambda^3 + b(k)\lambda^2 + c(k)\lambda + h(k) = 0,$$

where

$$(3.10a) \qquad\qquad b(k) = 2 + \gamma k^2 - \frac{1}{\alpha}\left(f_u + 2g_r\right) > 0,$$

$$(3.10b) \qquad c(k) = \frac{2}{\alpha^2} \left(f_u g_r - f_r g_u \right) - \frac{2}{\alpha} \left(f_u + 2g_r + \gamma g_r k^2 \right) + k^2 + 2\gamma k^2,$$

and

$$(3.10c) \qquad h(k) = \frac{4}{\alpha^2} \left(f_u g_r - f_r g_u \right) - \frac{k^2}{\alpha} \left(f_u + 4\gamma g_r \right) + \gamma k^4.$$

In general, for each value of k there will be three eigenvalues $\lambda_j(k)$, $j = 1, 2, 3$, one of which will be real and the other two either are real or form a complex conjugate pair. There are thus three solution branches or dispersion curves. Note, in particular, that in the limit $|k| \to \infty$, the three roots behave as $\lambda_1(k) \sim -k^2\gamma$, $\lambda_{2,3}(k) \sim \pm ik$.

We now determine conditions for the fixed point to become unstable with respect to non-oscillatory spatially periodic patterns. This means that a single real dispersion curve crosses zero from below, while the other pair of (possibly complex conjugate) branches have negative real parts for all k. A necessary condition is that there exists a wavenumber k for which there is a single real root $\lambda(k) = 0$. In order for this to hold, the λ-independent term in (3.9) must vanish, $h(k) = 0$, which implies

$$(3.11) \qquad k^2 = \frac{1}{2\alpha\gamma} \left(f_u + 4\gamma g_r \pm \sqrt{(f_u + 4\gamma g_r)^2 - 16\gamma \left(f_u g_r - f_r g_u \right)} \right).$$

There are then two conditions for (3.11) to have a real solution k: (1) the discriminant is positive, and (2) k^2 is positive. The first condition implies that

$$(3.12) \qquad (f_u + 4\gamma g_r)^2 > 16\gamma \left(f_u g_r - f_r g_u \right),$$

which certainly holds for sufficiently small γ. Positivity of k^2 then requires

$$(3.13) \qquad f_u + 4\gamma g_r > 0.$$

The condition (3.13) on γ depends on the sign of g_r, that is,

$$\gamma > -\frac{f_u}{4g_r}, \quad g_r > 0,$$

$$(3.14) \qquad \gamma < -\frac{f_u}{4g_r} \quad g_r < 0.$$

The first case, $g_r > 0$, implies that $f_u < 0$ due to condition (3.7a). On the other hand, if $g_r < 0$, then $f_u > 0$, since the condition $f_u < 0$ would imply that the positive quantity γ would be less than a negative quantity. We conclude that f_u and g_r must have opposite sign and, hence, f_r and g_u also have opposite sign; see (3.7b).

In general, there will be two positive roots k for which $\lambda(k) = 0$, suggesting that when the discriminant vanishes in (3.11) for some $\gamma = \gamma_c$ and $k = k_c$, the fixed point is marginally stable with respect to the Fourier mode $e^{ik_c x}$. However, in order to eliminate the possibility of a Turing–Hopf bifurcation, we must check that a pair of pure imaginary roots $\pm i\omega$ cannot

occur at some value of k. As we show below, this leads to the additional requirement that $g_r < 0$ and, hence, $f_u > 0$. Conditions (3.7a), (3.7b), and (3.14) then imply that

$$(3.15) \qquad \gamma < -\frac{f_u}{4g_r} < \frac{1}{2}, \quad g_r < 0, \quad f_u > 0, \quad f_r g_u < 0.$$

Setting $\lambda(k) = i\omega(k)$ in (3.9) for real $\omega(k)$ and equating real and imaginary parts generates the pair of equations

$$c(k) - \omega^2 = 0, \quad h(k) - b(k)\omega^2 = 0 \Rightarrow c(k)b(k) = h(k) > 0.$$

Writing $c(k)b(k) = a_0 + a_1 k^2 + a_2 k^4$ and $h(k) = h_0 + h_1 k^2 + h_2 k^4$, we find from (3.7a), (3.7b), (3.13) and $g_r < 0$ that $a_0 > b_0$, $a_1 > 0$, $h_1 < 0$, and $a_2 > h_2$ so $c(k)b(k) > h(k)$ for all k. In other words, a pair of complex conjugate roots cannot cross the imaginary axis. This result is a special case of a more general theorem due to Guckenheimer, Myers, and Sturmfels [9]. For completeness, we state the theorem here.

THEOREM (Guckenheimer, Myers, and Sturmfels). *Let* **S** *by the Sylvester matrix for the characteristic polynomial* $p(\lambda)$ *of an* $n \times n$ *matrix* Δ. *Then,* Δ *has precisely one pair of pure imaginary eigenvalues if* $\det(\mathbf{S}) = 0$ *and* $\det(\mathbf{S}_0) \cdot (\mathbf{S}_1) > 0$, *where* $\mathbf{S}_{i=0,1}$ *denotes the matrices obtain from* **S** *by deleting row 1 and* $n/2$ *and columns 1 and* $i + 2$. *If* $\det(\mathbf{S}) \neq 0$, *or* $\det(\mathbf{S}_0) \cdot \det(\mathbf{S}_1) < 0$, *then* $p(\lambda)$ *has no purely imaginary roots.*

For our $n = 3$ system the corresponding Sylvester matrix is

$$(3.16) \qquad \mathbf{S}(k) = \begin{pmatrix} h(k) & b(k) \\ c(k) & 1 \end{pmatrix},$$

and we have shown $\det(\mathbf{S}(k)) \neq 0$ for all k.

3.2. Dispersion curves. We now apply the above linear stability analysis to the modified GM reaction scheme given by (2.5). In the absence of spatial disturbances, the steady state for this model is

$$U^* = \frac{\mu_2}{\mu_1}, \quad R_+^* = R_-^* = \frac{\rho \mu_2}{2\mu_1^2},$$

so we have the following derivatives evaluated at steady state:

$$(3.17) \qquad f_u = 2\mu_1, \quad f_r = -\frac{\mu_1^2}{\rho}, \quad g_u = \frac{2\rho\mu_2}{\mu_1}, \quad g_r = -\mu_2.$$

For this model, the condition that f_u and g_r have opposite signs at steady state is already satisfied for any positive values of μ_1 and μ_2. To satisfy the remaining conditions (3.15) for stability in the homogeneous steady state, we require

$$f_u + 2g_r < 0 \Rightarrow \mu_1 < \mu_2$$

from (3.7a). Second,

$$f_u g_r - f_r g_u = 0$$

which is a limiting case of (3.7b). Thus, we have a (marginally) stable homogeneous steady state in the absence of spatial disturbances, provided that the inhibitor GLR-1 decays more
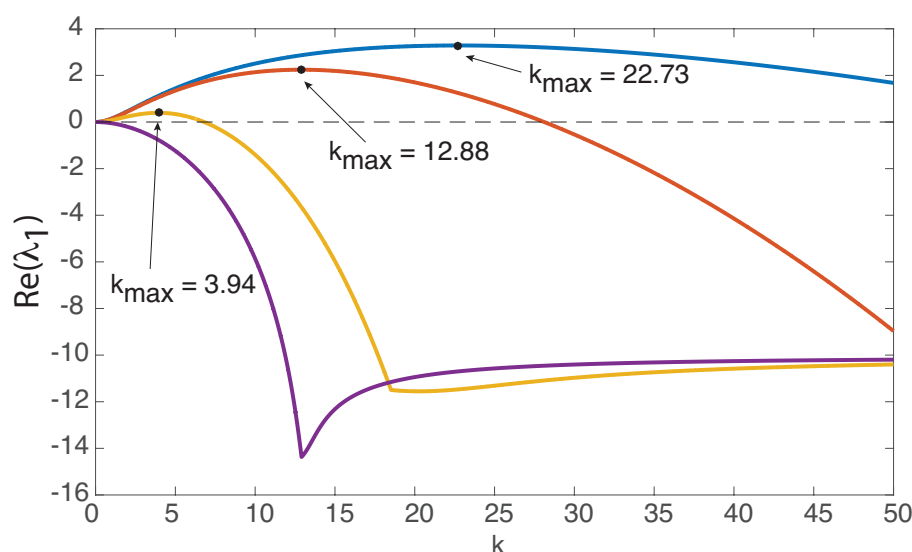
Figure 5. *Dispersion curves for the transport model* (2.3) *with modified GM kinetics* (2.5). *We choose* $\rho = 1, \mu_1 = 0.25, \mu_2 = 1, \alpha = 0.11,$ *and* $v = 1$ *in order to match biophysical parameters and satisfy the spatially homogeneous stability conditions.* λ_1 *represents the eigenvalue of the system with largest real part for a given* k. *We look at dispersion curves for four different values of* D: $D = 0.01$ *(blue),* $D = 0.05$ *(red),* $D = 0.5$ *(yellow),* $D = 1.5$ *(purple). The maximum value of* λ_1 *occurs at some value* $k_{\max}$, *which gives the dominant mode for pattern formation.*

quickly than the activator CaMKII. It remains to consider the necessary condition (3.15) on γ for a Turing instability to occur. In this case of the Gierer–Meinhardt model, the condition reads

$$\gamma < \frac{\mu_1}{2\mu_2} < \frac{1}{2}.$$

In Figure 5, we show the dispersion curves for the trafficking system with Gierer–Meinhardt nonlinearities. That is, we plot $\text{Re}[\lambda_1]$ against wavenumber k, where λ_1 is the eigenvalue with largest real part. One finds that in any region where $\text{Re}[\lambda_1] > 0$, λ_1 is real, thus signaling the growth of nonoscillatory spatially periodic patterns, with the maximum of the curve representing the fastest growing mode. As γ increases (i.e., either D increases or v decreases), instabilities disappear as predicted by the theory. Figure 6 shows a numerically simulated example of pattern formation in the 1D trafficking system with Gierer–Meinhardt dynamics. The corresponding time evolution of the pattern is illustrated in Figure 7.

3.2.1. Parameter values. In order to justify the trafficking-based mechanism for pattern formation in *C. elegans*, the conditions for Turing instability must be satisfied for biophysically relevant parameters. Many of these parameters can be cited from the biological literature. First, we note that the conditions for stability in the homogeneous steady state are satisfied in this system because the decay rate of GLR-1 is approximately four times that of CaMKII [13, Table 1]. For our simulations, we take $\mu_1 = 0.25/s$ and $\mu_2 = 1/s$. Additionally, there exists data on the transport of GLR-1 via molecular motors. The average velocity of GLR-1
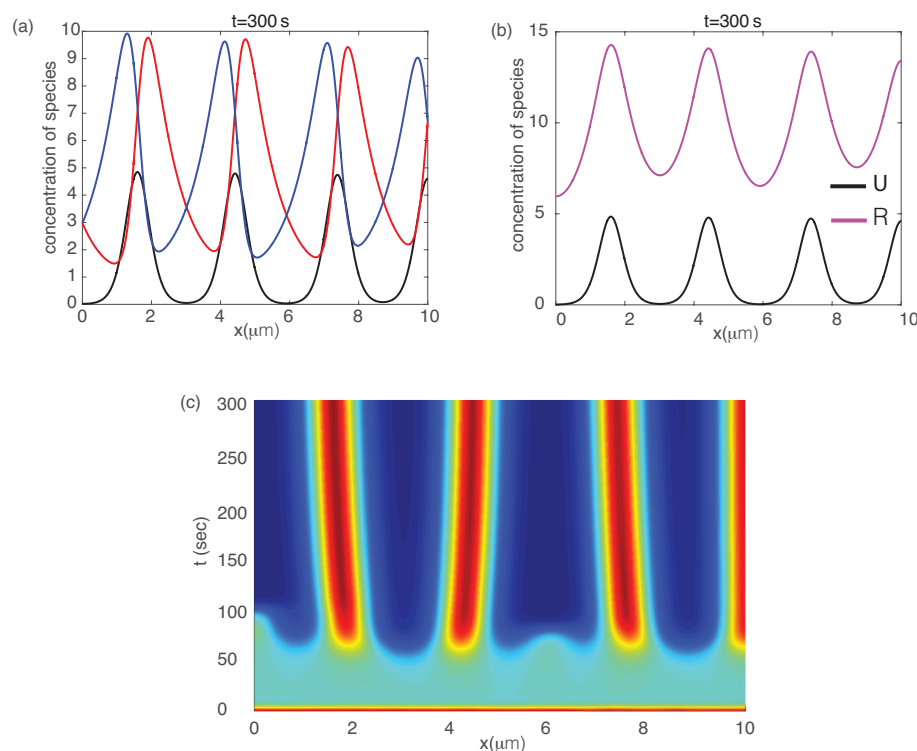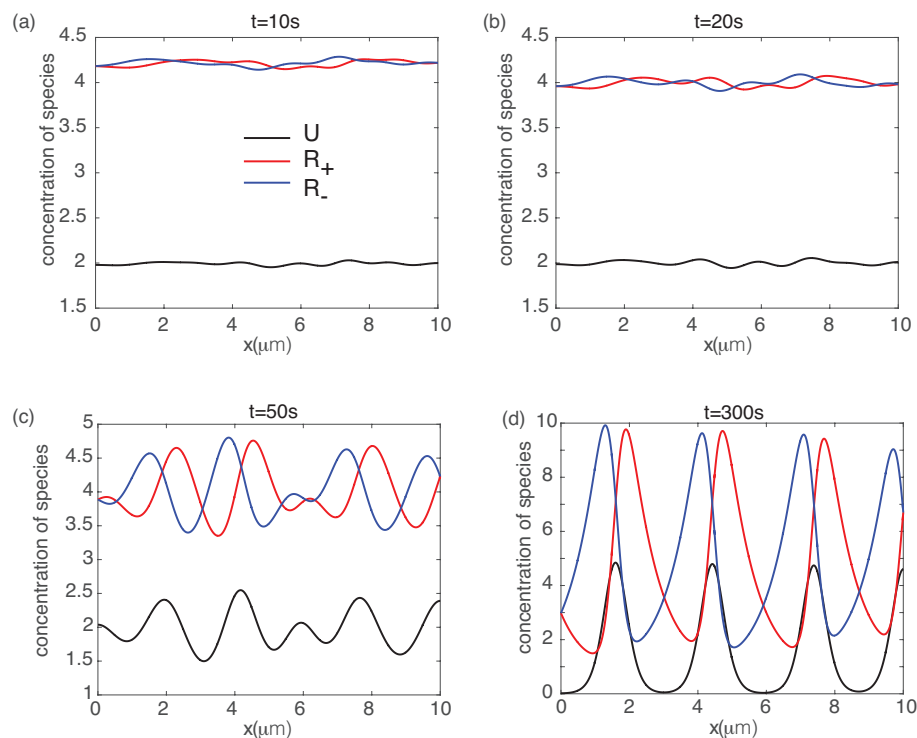
Figure 6. *Synapse site pattern formation in* C. elegans *active transport model.* (a) *Spatial profiles of the steady-state concentration of components* $U, R_{\pm}$. (b) *Another example of spatial profiles showing that* U *and* $R = R_{+} + R_{-}$ *are in-phase. Initial data are generated from a uniform random distribution. Nonlinearity parameters are the same as in Figure* 5, *with* $D = 0.01\ \mu m^2/s$. (c) *Full solution in space and time. Colors represent concentrations of GLR-*1 $= R_{+} + R_{-}$, *with red representing areas of highest concentration. Our simulation shows the emergence of* ~ 4 *synapse sites in* 10 μm. *In this and subsequent figures, simulations were performed using a Crank–Nicolson scheme for* U *and a Lax–Wendroff scheme for* $R_{\pm}$ *with time step* $dt = 0.005$, *space step* $dx = 0.01$, *and no-flux boundary conditions.*

undergoing active transport along the ventral cord is 1 μm/s, with an average run length of 9.2 μm [19]. From this, we can infer that our switching rate should be $\alpha \approx 0.11/s$.

We begin with concentrations chosen from a uniform random distribution near fixed point values. As the system evolves, we initially observe growth of CAMKII concentrations, and then patterns emerge as the activator is eventually tempered by increase of the inhibitor GLR-1. In this case, the concentration of both activating and inhibiting species are in phase with each other. In order to test the validity of our mechanism, we seek to match data due to Rongo and Kaplan [26], which show that *C. elegans* synaptic density is fixed at 3.7 ± 0.1 per 10 μm. With the parameter values discussed here, our numerical simulations show good agreement with the biophysical system, with $\sim$4 potential synapse sites per 10 μm (see Figure 6).

3.3. The reaction-diffusion limit. At first sight it could be argued that the occurrence of a Turing instability in the active transport model (2.3) is not surprising since it is well known that in the fast switching limit $\alpha \to \infty$ the transport model reduces to a two-component reaction-diffusion system [21]. However, recall from (3.2) that three quantities make up the

Figure 7. *Time evolution of synapse site pattern formation in* C. elegans *active transport model. Each plot shows the concentration of species* $U, R_\pm$ *as a function of* x *for a specific time* t*. Initial data are generated from a uniform random distribution. Nonlinearity parameters are the same as in Figure* 5 *with* $D = 0.01$ $\mu m^2/s$*.*

dimensionless bifurcation parameter γ: v, D, and α. We have shown that γ has to be sufficiently small for pattern formation to occur in the active transport model. That is, in the limit of fast switching we have $v^2/D \ll \alpha$, which suggests that the effective diffusive transport of the inhibitor GLR-1 is much slower than the activator CaMKII. Since the occurrence of a Turing instability in a reaction-diffusion model with GM kinetics requires fast inhibition and slow activation [18, 20], we expect pattern formation to disappear in the fast switching limit, which is indeed found to be the case.

In order to explore this issue in a little more detail, we apply a quasi-steady-state diffusion approximation to the linearized version of (2.3) along the lines of [21]. First, we set $\alpha = \alpha_0/\epsilon$, where $\epsilon << 1$ is chosen so that $\alpha_0 = \mathcal{O}\left(v^2/D\right)$. We then rewrite the original system (2.3), linearized about the fixed point, as

$$(3.18) \qquad \boldsymbol{u}_t = \mathbf{D}\boldsymbol{u}_{xx} + \mathbf{V}\boldsymbol{u}_x + \frac{\alpha_0}{\epsilon}\mathbf{A}\boldsymbol{u} + \mathbf{B}\boldsymbol{u},$$

where $\boldsymbol{u} = \begin{pmatrix} u & r & l \end{pmatrix}^T$ and

$$\mathbf{D} = \begin{pmatrix} D & 0 & 0 \\ 0 & 0 & 0 \\ 0 & 0 & 0 \end{pmatrix}, \quad \mathbf{V} = \begin{pmatrix} 0 & 0 & 0 \\ 0 & -v & 0 \\ 0 & 0 & v \end{pmatrix},$$

$$\mathbf{A} = \begin{pmatrix} 0 & 0 & 0 \\ 0 & -1 & 1 \\ 0 & 1 & -1 \end{pmatrix}, \quad \mathbf{B} = \begin{pmatrix} f_u & f_r & f_r \\ g_u & g_r & g_r \\ g_u & g_r & g_r \end{pmatrix}.$$

Note that the symmetric matrix $\mathbf{A}$ has a 2D nullspace ϕ spanned by

$$\left\{ \phi_1 = \begin{pmatrix} 1 \\ 0 \\ 0 \end{pmatrix}, \phi_2 = \frac{1}{\sqrt{2}} \begin{pmatrix} 0 \\ 1 \\ 1 \end{pmatrix} \right\},$$

with $\langle \phi_i, \phi_j \rangle = \delta_{ij}$ In order to separate the timescales and perform the quasi-steady-state reduction, we introduce the decomposition

$$(3.19) \qquad \boldsymbol{u}(x,t) = \sum_{i=1,2} C_i(x,t)\phi_i(x,t) + \epsilon \boldsymbol{w}(x,t),$$

where $C_i(x,t) = \langle \phi_i, \boldsymbol{u} \rangle$. We observe two things about this decomposition: first, $C_i(x,t)$ is a projection, into the nullspace of $\mathbf{A}$, and second, w must be orthogonal to the nullspace of $\mathbf{A}$ so $\boldsymbol{w} = (w/\sqrt{2}) \left((0,1,-1)^\top \right)$. Substituting (3.19) into (3.18) yields

$$\frac{\partial}{\partial t} \left[\sum_{i=1,2} C_i \phi_i \right] + \epsilon \frac{\partial \boldsymbol{w}}{\partial t} = \alpha_0 \mathbf{A} \boldsymbol{w} + \sum_{i=1,2} C_i \mathbf{B} \phi_i + \frac{\partial C_2}{\partial x} \mathbf{V} \phi_2 + \frac{\partial^2 C_1}{\partial x^2} \mathbf{D} \phi_1$$

$$(3.20) \qquad\qquad + \epsilon \left(\mathbf{B} \boldsymbol{w} + \mathbf{V} \frac{\partial \boldsymbol{w}}{\partial x} + \mathbf{D} \frac{\partial^2 \boldsymbol{w}}{\partial x^2} \right).$$

We project onto the slow manifold by multiplying by ϕ_i^T to give

$$\frac{\partial C_1}{\partial t} = \sum_{i=1,2} C_i \phi_1^T \mathbf{B} \phi_i + d \frac{\partial^2 C_1}{\partial x^2} + \epsilon \phi_1^T \left(\mathbf{B} \boldsymbol{w} + \mathbf{D} \frac{\partial^2 \boldsymbol{w}}{\partial x^2} \right),$$

$$\frac{\partial C_2}{\partial t} = \sum_{i=1,2} C_i \phi_2^T \mathbf{B} \phi_i + \epsilon \left(\phi_2^T \mathbf{B} \boldsymbol{w} + \phi_2^T \mathbf{V} \frac{\partial \boldsymbol{w}}{\partial x} \right).$$

Note that $\mathbf{B}\boldsymbol{w} = 0$ and $\mathbf{D}\boldsymbol{w} = 0$. Next, we plug the slow equations into (3.20) to obtain an equation for w. After an application of the Fredholm alternative theorem we find that to leading order

$$(3.21) \qquad \boldsymbol{w} = \frac{v}{2\alpha_0} \begin{pmatrix} 0 \\ -1 \\ 1 \end{pmatrix} \frac{\partial C_2}{\partial x}.$$

Finally, we obtain the desired slow manifold equations by substituting in this leading order approximation for $\boldsymbol{w}$ and simplifying. Doing so leaves us with the reduced system

$$(3.22) \qquad \frac{\partial C_1}{\partial t} = f_u C_1 + \sqrt{2} f_r C_2 + D \frac{\partial^2 C_1}{\partial x^2},$$

$$(3.23) \qquad \frac{\partial C_2}{\partial t} = \sqrt{2} g_u C_1 + 2 g_r C_2 + \epsilon \frac{v^2}{\sqrt{2}\alpha_0} \frac{\partial^2 C_2}{\partial x^2}.$$

A in the full model (2.3), stability of the zero solution with respect to spatially uniform perturbations is ensured by conditions (3.7a) and (3.7b). Let $D_1 = D$ and $D_2 = \epsilon v^2 / \sqrt{2} \alpha_0$. A standard analysis of reaction diffusion systems leads to the following necessary condition for a Turing instability [20]:

$$(3.24) \qquad D_2 f_u + 2 D_1 g_r > 0.$$

When this is combined with the conditions $f_u + 2g_r < 0$, $f_u > 0$, and $g_r < 0$, we deduce that a necessary condition for a Turing instability is $D_2 > D_1$. This clearly cannot hold in the small ϵ limit (fast switching). This establishes that in the regime where bidirectional active transport effectively reduces to diffusion, a Turing instability cannot occur.

4. Biased active transport. So far we have assumed that the switching rates and speeds are the same for left-moving and right-moving particles. Now suppose that the speeds of the right-moving and left-moving states are v_r and v_l, respectively, with $v_l < v_r$. The mean speed of the active particles is then $\bar{v} = (v_r - v_l)/2$ and there is an additional advection term $-\bar{v} \partial C_2 / \partial x$ on the right-hand side of (3.23). We thus obtain a linearized version of an RDA system. There is a growing literature on pattern formation in 1D RDA equations, where one typically considers a finite or semi-infinite domain with some form of forcing at one end ($x = 0$, say) [28, 29, 30, 37]. The combination of forcing, advection, diffusion, and nonlinear reactions can lead to so-called stationary FDS. This suggests that we look for the analogue of an FDS in a biased version of our three-component trafficking model. The nondimensionalized equations with $v_r = v$ and $v_l = \nu v$ become (after rescaling)

$$(4.1a) \qquad \frac{\partial U}{\partial t} = \gamma \frac{\partial^2 U}{\partial x^2} + \frac{1}{\alpha} f(U, R_+, R_-),$$

$$(4.1b) \qquad \frac{\partial R_+}{\partial t} = -\frac{\partial R_+}{\partial x} + R_- - R_+ + \frac{1}{\alpha} g(U, R_+, R_-),$$

$$(4.1c) \qquad \frac{\partial R_-}{\partial t} = \nu \frac{\partial R_-}{\partial x} + R_+ - R_- + \frac{1}{\alpha} g(U, R_+, R_-),$$

where now we take $x \in [0, \infty)$ with the following boundary conditions at $x = 0$ [30]:

$$(4.2) \qquad U(0, t) = U^* + \epsilon_u(t), \quad R_+(0, t) = R_+^* + \epsilon_r(t), \quad R_-(0, t) = R_-^* + \epsilon_l(t),$$

for any $t > 0$, where

$$(4.3) \qquad \epsilon_i(t) = \begin{cases} \epsilon_i & \text{if } 0 \leq t \leq T, \\ 0 & \text{otherwise,} \end{cases}$$

and $\epsilon_i, |\epsilon_i| \ll 1$ for $i = u, r, l$ are small constant perturbations that are maintained for a long but finite time T. Here $\mathbf{u}^* = (u^*, r^*, l^*)$ is the spatially uniform steady state. Linearizing about this steady-state solution leads to (3.3) with the same matrices $\mathbf{A}$ and $\mathbf{D}$, and the modified matrix

$$\mathbf{J} = \begin{pmatrix} 0 & 0 & 0 \\ 0 & -1 & 0 \\ 0 & 0 & \nu \end{pmatrix}.$$

Equation (3.3) is supplemented by the boundary conditions

$$(4.4) \qquad u(0,t) = \epsilon_u(t), \quad r(0,t) = \epsilon_r(t), \quad l(0,t) = \epsilon_l(t),$$

Since the time-dependent perturbations have compact support in time, they have well-defined Fourier transforms. Therefore, we seek the general solution of (3.3) of the form [30]

$$(4.5) \qquad (u(x,t), r(x,t), l(x,t)) = \int_{-\infty}^{\infty} (u_0(\omega), r_0(\omega), l_0(\omega)) \epsilon^{i\omega t + z(\omega)x} d\omega,$$

where $u_0(\omega)$, etc., are determined by the boundary data. Substituting the general solution into (3.3) shows that (ω, z) must satisfy the characteristic equation

$$
\begin{aligned}
0 = &-(i\omega)^3 + (i\omega)^2 \left((\nu - 1)z - 2 + \gamma z^2 + \frac{1}{\alpha} (f_u + 2g_r) \right) \\
&+ i\omega \left(\frac{2}{\alpha^2} (\Delta) + \frac{2}{\alpha} \left(f_u + 2g_r - \gamma g_r z^2 \right) + \nu z^2 + 2\gamma z^2 \right. \\
&\left. - (\nu - 1)z \left[-1 + z^2 \gamma + \frac{f_u + g_r}{\alpha} \right] \right) \\
&+ \frac{4}{\alpha^2} (\Delta) - \frac{z^2}{\alpha} (\nu f_u + 4\gamma g_r) - \gamma \nu z^4 \\
(4.6) \qquad &+ (\nu - 1)z \left[\frac{-\Delta}{\alpha^2} - \gamma z^2 - \frac{f_u - \gamma z^2 g_r}{\alpha} \right].
\end{aligned}
$$

For notational convenience, we let $\Delta = f_r g_u - f_u g_r$. A necessary condition for a stationary-space periodic solution is that the ω-independent term in (4.6) vanishes:

$$
\begin{aligned}
&\gamma \nu z^4 + \gamma(\nu - 1) \left(1 - \frac{g_r}{\alpha} \right) z^3 + \frac{z^2}{\alpha} (\nu f_u + 4\gamma g_r) \\
(4.7) \qquad &- (\nu - 1)z \left[\frac{-\Delta}{\alpha^2} - \frac{f_u}{\alpha} \right] - \frac{4}{\alpha^2} \Delta = 0.
\end{aligned}
$$

Solutions that bifurcate to spatially periodic FDS have a purely imaginary wavenumber $z_c = ik_c$. The vanishing of the imaginary part of (4.7) when $z = ik_c$ shows that the critical wavenumber is

$$(4.8) \qquad k_c^2 = \frac{\alpha f_u + \Delta}{\alpha \gamma (\alpha - g_r)},$$

which exists provided that the right-hand side is positive. Note that k_c is independent of the speed bias ν.

We can now determine the neutral curve in (γ, ν) parameter space for the boundary-forcing problem that corresponds to the bifurcation to stationary (FDS) solutions by requiring that the real part of (4.7) vanishes when $z = ik_c$ and solving for ν:

$$(4.9) \qquad \nu^*(\gamma) = \frac{4 \left(\Delta + \alpha \gamma g_r k_c^2(\gamma) \right)}{\alpha k_c^2(\gamma) \left(\alpha \gamma k_c^2(\gamma) - f_u \right)}.$$
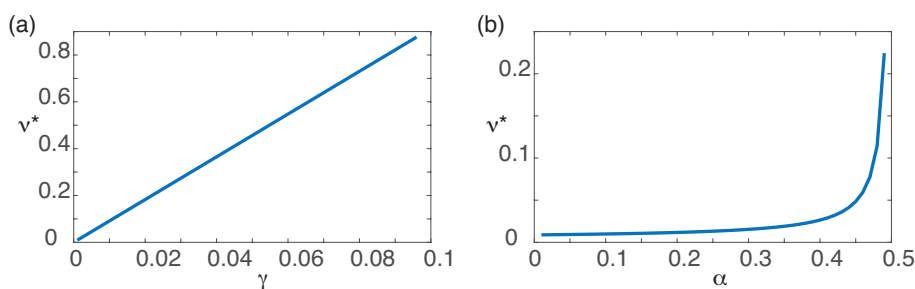
Figure 8. *Plot of* (a) *the* (α, ν^*) *and* (b) *the* (γ, ν^*) *curves for the Gierer–Meinhardt synaptogenesis model with biased active transport. We predict pattern forming instabilities to arise for regions where* $\nu > \nu^*$. *For the Gierer–Meinhardt model, we take nonlinearity parameters* $\rho = 1, \mu_1 = 0.25, \mu_2 = 1$.

We can further simplify this by plugging in our expression for k_c^2,

$$(4.10) \qquad \nu^*(\gamma) = \frac{4\gamma\alpha\,(\alpha - g_r)}{\alpha f_u + \Delta},$$

provided $\alpha - g_r \neq 0$ and $\alpha f_u + \Delta \neq 0$. In seeking stationary FDS solutions, we require that $k_c^2 > 0$ and $\nu^*(\gamma) > 0$. We predict that for ν above this curve defined by ν^*, we will see such solutions. We restrict our analysis here to the case we have explored previously, namely, the Gierer–Meinhardt model. Figure 8 shows the neutral curves in (γ, ν) and (α, ν) parameter space. Since $g_r < 0$, we know that $\alpha - g_r > 0$. This implies that we have the following condition for $k_c^2 > 0$:

$$(4.11) \qquad \alpha f_u + \Delta > 0.$$

We show examples of pattern formation in this biased transport regime in Figure 9 for the Gierer–Meinhardt model under multiple values of $\nu > \nu^*$. These patterns arise due to instability and persist in time, despite the underlying net flow to the right. However, we remark here that for certain parameter values, it is possible to generate transient convective instabilities, where the emergent patterns are eventually convected away from their initial perturbation and out of the domain in long times [27, 32]. Further explorations of types of instabilities and conditions under which they arise are not explored in the present work, but yield interesting opportunities for future analysis. Finally, it is important to note that, as in the case of Turing instabilities, FDS solutions do not occur in the fast switching limit for which biased bidirectional transport reduces to advection-diffusion.

5. Discussion. In summary, we have established the existence of an active trafficking-based mechanism for Turing pattern formation in a simple 1D model of synaptogenesis in *C. elegans*. Our model assumes that synaptogenesis is generated by an activator-inhibitor system consisting of passively diffusing Ca^{2+}/calmodulin-dependent protein kinase (CAMKII) and actively transported glutamate receptor 1 (GLR-1). Interactions between the two chemical species were modeled in terms of modified GM kinetics. We used linear stability analysis to derive conditions for a Turing instability and found that $\gamma = \alpha D/v^2$ has to be sufficiently small for patterns to emerge, where α is the motor switching rate, D is the CaMKII diffusion coefficient, and v is the speed of motor-driven GLR-1. One consequence is that patterns
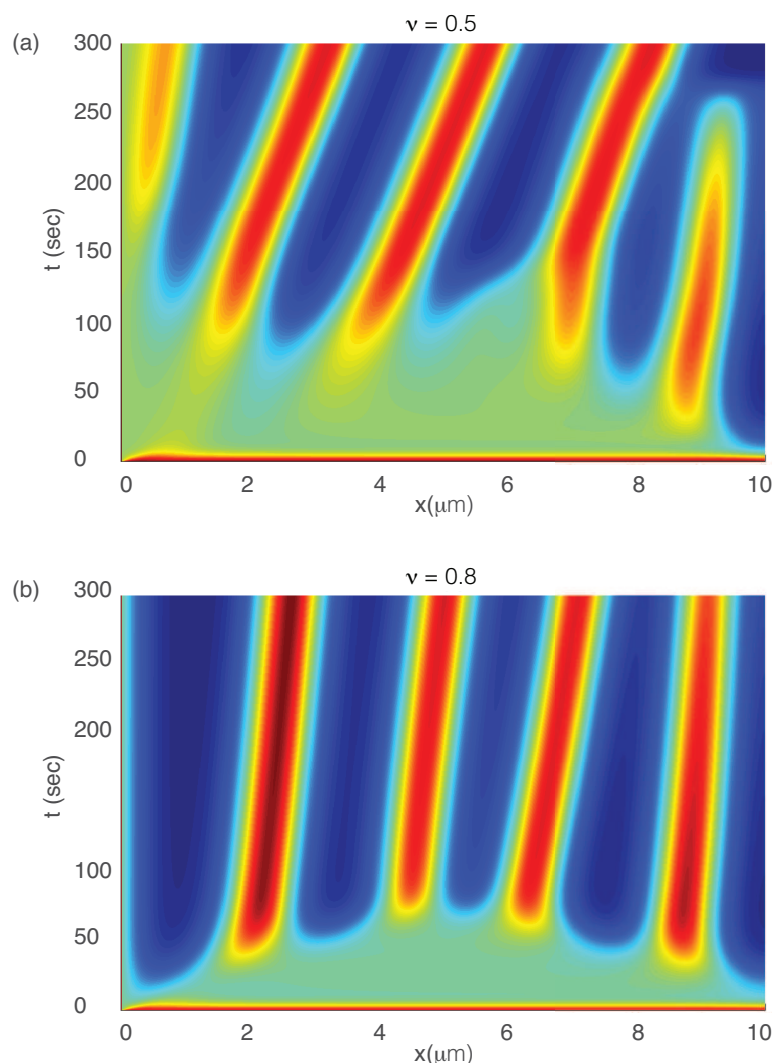
Figure 9. *Examples of evolution of patterns in the Gierer–Meinhardt model under biased active transport. We show two different values of $\nu > \nu^*$: (a) $\nu = 0.5$ and (b) $\nu = 0.8$. We take $\rho = 1, \mu_1 = 0.25, \mu_2 = 1, \gamma = 0.0011$, and $\alpha = .11$, as in Figure 8. Despite a biasing in anterograde versus retrograde transport speeds, the density of potential synaptic sites is still properly regulated. Note that despite a net flow to the right, patterns persist in long times (as opposed to being convected out of the domain). Numerical simulations were performed with the Crank–Nicolson scheme for diffusion and Lax–Wendroff scheme for advection with $\Delta x = 0.01$ and $\Delta t = 0.005$. We take Dirichlet boundary conditions on the left and no flux boundary conditions on the right.*

emerge outside the parameter regime of fast switching, where the linearized model reduces to a two-component reaction-diffusion system. In the case of GM kinetics, the spatially periodic densities for CaMKII and GLR-1 were in-phase, consistent with the interpretation of regions with enhanced densities corresponding to regularly spaced synaptic sites. Moreover, for physiologically reasonable choices of various biophysical parameters such as the diffusivity, motor speed, and degradation rates, the resulting synaptic spacing (pattern wavelength) is
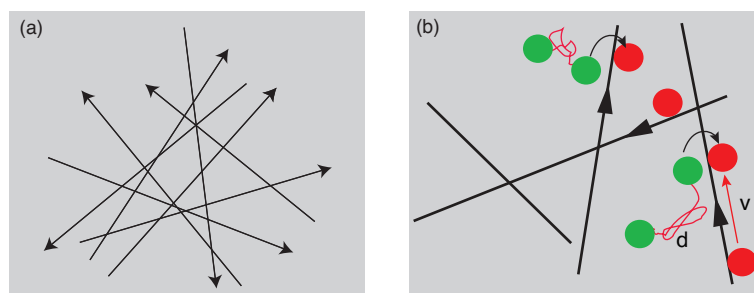
consistent with experimental data. Our results were also robust to changes in these parameters and persisted in the case of biased transport.

Further evidence for our hypothesis that synaptogenesis arises via a Turing mechanism is the observation that the spacing between synapses is maintained during larval growth [26]. In the case of reaction-diffusion equations, the role of domain growth in pattern formation has been investigated by a number of authors [35, 5, 24, 4, 6]. Much of this work has been inspired by experimental observations concerning the skin pigmentation of the marine angelfish [15]. In juvenile fish, the skin color is initially gray and then develops alternating white stripes on a dark blue background. New white stripes are inserted between the existing older stripes, resulting in a doubling of the number of stripes each time the fish doubles in size. Stripe insertion has also been modeled within the context of ocular dominance columns within developing cortex [23]. In the case of synaptogenesis in *C. elegans*, maintenance of synaptic density could be analogous to a stripe insertion mechanism and is something we hope to explore in future work. We will also develop a more detailed multicomponent model that explicitly distinguishes between cytoplasmic and membrane-bound densities.

Another possible extension of our work would be to analyze the generation of patterns in higher spatial dimensions. In the case of axonal or dendritic transport in neurons, microtubules tend to be aligned in parallel so that one can treat the transport process as effectively 1D. On the other hand, intracellular transport within the cell body of neurons and most nonpolarized animal cells occurs along a microtubular network that projects radially from organizing centers (centrosomes) with outward polarity. This allows the delivery of cargo to and from the nucleus. It has also been found that microtubules bend due to large internal stresses, resulting in a locally disordered network. A detailed microscopic model of intracellular transport within the cell would need to specify the spatial distribution of microtubular orientations and polarity, in order to determine which velocity states are available to a motor-cargo complex at a particular spatial location. However, a simplified model can be obtained under the "homogenization" assumption that the network is sufficiently dense so that the set of velocity states (and associated state transitions) available to a motor complex is independent of position. In that case, one can effectively represent the active transport within the cell in terms of a 2D or 3D model of active transport [2, 3].

For the sake of illustration, consider a disordered 2D microtubular network as illustrated in Figure 10. We assume that ATs are transported along this network, randomly switching between different motile states, and interacting with a second chemical species passively transported particles (PT) undergoing 2D diffusion. Suppose that after homogenization, an AT at any point $\mathbf{r} = (x, y)$ in the plane can exhibit ballistic motion with velocity $\mathbf{v}(\theta) = v(\cos\theta, \sin\theta)$ for $\theta \in [0, 2\pi)$ or be in a stationary state. Transitions between different ballistic states are governed by a discrete Markov process with θ-independent transition rate α. Let $c(\mathbf{r}, \theta, t)$ be the concentration of ATs in state $(\mathbf{r}, \theta)$ at time t and $u(\mathbf{r}, t)$ denote the concentration of PT. The 2D analogue of (2.3) is taken to be

$$\frac{\partial u}{\partial t} = d\nabla^2 u + f(u, C),$$
$$\frac{\partial c}{\partial t} = -\nabla \cdot (\mathbf{v}(\theta)c) - \alpha c(\mathbf{r}, \theta, t) + \alpha C(\mathbf{r}, t) + g(u, C),$$

Figure 10. *Active transport on a disordered microtubular network.* (a) *Random orientational arrangement of microtubules.* (b) *Effective* 2D *trajectory of an AT (red) randomly switching directions and reacting with the ATs (green).*

where

$$C(\mathbf{r}, t) = \frac{1}{2\pi} \int_0^{2\pi} c(\mathbf{r}, \theta', t) d\theta'.$$

Alternatively, one could take $g(u, c)$ rather than the more symmetric case of $g(u, C)$.

Finally, the new class of model introduced in this paper raises many interesting questions from a mathematical perspective. First, we are considering coupled hyperbolic and parabolic nonlinear PDEs — what are the conditions for well-posedness (existence, uniqueness, stability) for such equations? Second, we focused on the issue of linear stability in order to derive necessary conditions for a Turing instability. However, if one wants to determine the selection and stability of the emerging patterns, it is necessary to take into account the nonlinearities of the system using methods such as weakly nonlinear analysis. This then raises a third issue, namely, the role of symmetry in the selection of patterns. This is a well-studied area in the case of reaction-diffusion systems with an underlying Euclidean symmetry [14]. An additional complicating feature of our trafficking model is that a 2D or 3D microtubular network tends to break Euclidean symmetry, and this depends on the spatial scale at which one is modeling.

REFERENCES

[1] M. ALBER, H. G. E. HENTSCHEL, B. KAZMIERCZAK, AND S. A. NEWMAN *Existence of solutions to a new model of biological pattern formation*, J. Math. Anal. Appl., 308 (2004), pp. 175–194.

[2] O. BENICHOU, C. LOVERDO, M. MOREAU, AND R. VOITURIEZ, *Intermittent search strategies*, Rev. Mod. Phys., 83 (2011), pp. 81–129.

[3] P. C. BRESSLOFF, *Stochastic Processes in Cell Biology*, Springer, New York, 2014.

[4] M. A. J. CHAPLAIN, M. GANESH, AND I. G. GRAHAM, *Spatio-temporal pattern formation on spherical surfaces: Numerical simulation and application to solid tumor growth*, J. Math. Biol., 42 (2001), pp. 387–423.

[5] E. J. CRAMPIN, E. A. GAFFNEY, AND P. K. MAINI, *Reaction and diffusion on growing domains: Scenarios for robust pattern formation*, Bull. Math. Biol., 61 (1999), pp. 1093–1120.

[6] E. J. CRAMPIN, E. A. GAFFNEY, AND P. K. MAINI. *Mode-doubling and tripling in reaction-diffusion patterns on growing domains: A piecewise linear model*, J. Math. Biol., 44, (2002), pp. 107–128.

[7] L. EDELSTEIN-KESHET, *Mathematical Models in Biology*, Classics in Appl. Math. 46, SIAM, Philadelphia, 1988.

[8] A. GIERER AND H. MEINHARDT, *A theory of biological pattern formation*, Kybernetik, 12 (1972), pp. 30–39.

[9] J. GUCKENHEIMER, M. MYERS, AND B. STURMFELS, *Computing Hopf bifurcations* I, SIAM J. Numer. Anal., 34 (1997), pp. 1–21.

[10] A. K. HARRIS, P. WARNER, AND D. STOPAK, *Generation of spatially periodic patterns by a mechanical instability: A mechanical alternative to the Turing model*, Development, 80 (1984), pp. 1–20.

[11] F. J. HOERNDLI, D. A. MAXFIELD, P. J. BROCKIE, J. E. MELLEM, E. JENSEN, R. WANG, D. M. MADSEN, AND A. V. MARICQ. *Kinesin-1 regulates synaptic strength by mediating the delivery, removal, and redistribution of AMPA receptors.* Neuron, 80 (2013), pp. 1421–1437.

[12] F. J. HOERNDLI, R. WANG, J. E. MELLEM, A. KALLARACKAL, P. J. BROCKIE, C. THACKER, E. JENSEN, D. M. MADSEN, AND A. V. MARICQ. *Neuronal activity and CaMKII regulate kinesin-mediated transport of synaptic AMPARs.* Neuron, 86 (2015), pp. 457–474.

[13] C. HANUS AND E. M. SCHUMAN, *Proteostasis in complex dendrites*, Nature Rev. Neurosci., 14 (2013), pp. 638–648.

[14] R. B. HOYLE, *Pattern Formation: An Introduction to Methods*, Cambridge University Press, Cambridge, UK, 2006.

[15] S. KONDO AND R. ASAI, *A reaction–diffusion wave on the skin of the marine angelfish* pomacanthus, Nature, 376, (1995) pp. 765–768.

[16] A. J. KOCH AND H. MEINHARDT, *Biological pattern formation: From basic mechanisms to complex structures*, Rev. Mod. Phys., 66 (1994), p. 1481.

[17] S. K. KONDO AND T. MIURA, *Reaction-diffusion model as a framework for understanding biological pattern formation*, Science, 329 (2010), pp. 1616–1620.

[18] H. MEINHARDT, *Models of Biological Pattern Formation*, Vol. 6, Academic Press, London, 1982.

[19] M. I. MONTEIRO, S. AHLAWAT, J. R. KOWALSKI, E. MALKIN, S. P. KOUSHIKA, AND P. JUOA, *The kinesin-3 family motor KLP-4 regulates anterograde trafficking of GLR-1 glutamate receptors in the ventral nerve cord of Caenorhabditis elegans*, Mol. Biol. Cell. 23 (2012), pp. 3647–3662.

[20] J. D. MURRAY, *Mathematical Biology. II Spatial Models and Biomedical Applications*, Interdiscip. Appl. Math. 18, Springer-Verlag, New York, 2001.

[21] J. M. NEWBY AND P. C. BRESSLOFF, *Quasi-steady state reduction of molecular motor-based models of directed intermittent search*, Bull. Math. Biol., 72 (2010), pp. 1840–1866.

[22] G. NICOLIS AND I. PRIGOGINE, *Self-Organization in Nonequilibrium Systems*, Wiley-Interscience, New York, 1977.

[23] A. M. OSTER AND P. C. BRESSLOFF, *A developmental model of ocular dominance formation on a growing cortex*, Bull. Math. Biol., 68, (2006), pp. 73–98.

[24] K. J. PAINTER, P. K. MAINI, AND H. G. OTHMER, *Stripe formation in juvenille* Pomacathus *explained by a generalized Turing mechanism with chemotaxis*, Proc. Natl. Acad. Sci. USA, 96 (1999), pp. 5549–5554.

[25] E. M. RAUCH AND M. M. MILLONAS, *The role of trans-membrane signal transduction in Turing-type cellular pattern formation*, J. Theoret. Biol. 226 (2004), pp. 401–407.

[26] C. RONGO AND J. M. KAPLAN, *CaMKII regulates the density of central glutamatergic synapses in vivi,* Nature, 402 (1999), pp. 195–199.

[27] B. SANDSTEDE AND A. SCHEEL, *Absolute and convective instabilities of waves on unbounded and large bounded domains,* Phys. D, 145 (2000), pp. 233–277.

[28] R. A. SATNOIANU, M. MENZINGER, AND P. K. MAINI, *Turing instabilities in general systems,* J. Math. Biol., 41 (2000), pp. 493–512.

[29] R. A. SATNOIANU AND M. MENZINGER, *Non-Turing stationary patterns in flow-distributed oscillators with general diffusion and flow rates,* Phys. Rev. E, 62 (2000), pp. 113–119.

[30] R. A. SATNOIANU, P. K. MAINI, AND M. MENZINGER, *Parameter space analysis, pattern sensitivity and model comparison for Turing and stationary flow-distributed waves (FDS),* Phys. D, 160 (2001), pp. 79–102.

[31] K. SHEN AND T. MEYER, *Dynamic control of CaMKII translocation and localization in hippocampal neurons by NMDA receptor stimulation*, Science, 284 (1999), pp. 162–166.

[32] J. A. SHERRATT, A. S. DAGBOVIE, AND F. M. HILKER, *A mathematical biologists guide to absolute and convective instability*, Bull. Math Biol., 76 (2014), pp. 1–26.

[33] N. V. SWINDALE, *A model for the formulation of ocular dominance stripes*, Proc. R. Soc. Lond. B, 208 (1980), pp. 243–264.

[34] A. M. Turing, *The chemical basis of morphogenesis*, Philos. Trans. Roy. Soc. Lond. Ser. B Biol. Sci., 237 (1952), pp. 37–72.

[35] C. Varea, J. L. Aragon, and R. A. Barrio, *Confined Turing patterns in growing systems*, Phys. Rev. E, 56 (1997), pp. 1250–1253.

[36] M. Yamaguchi, E. Yoshimoto, and S. Kondo, *Pattern regulation in the stripe of zebrafish suggests an underlying dynamic and autonomous mechanism*, Proc. Natl. Acad. Sci. USA, 104 (2007), pp. 4790–3.

[37] A. Yochelis and M. Sheintuch, *Principal bifurcations and symmetries in the emergence of reaction-diffusion-advection patterns on finite domains,* Phys. Rev. E, 80 (2009), 056201.